J|A|C|S ARTICLES

Published on Web 10/12/2010

Synthesis of Metal−Hydrazone Complexes and Vapochromic Behavior of Their Hydrogen-Bonded Proton-Transfer Assemblies

Atsushi Kobayashi,*,† Masa-aki Dosen,† Mee Chang,† Kiyohiko Nakajima,‡ Shin-ichiro Noro,§ and Masako Kato*,†

Department of Chemistry, Faculty of Science, Hokkaido University, North-10 West-8, Kita-ku, Sapporo 060-0810, Japan, Department of Chemistry, Aichi University of Education, Igaya, Kariya, Aichi 448-8542, Japan, and Research Institute for Electronic Science, Hokkaido University, North-20 West-10, Kita-ku, Sapporo 001-0020, Japan

Received July 17, 2010; E-mail: akoba@sci.hokudai.ac.jp; mkato@sci.hokudai.ac.jp

Abstract: We synthesized and investigated a new series of metal−hydrazone complexes, including deprotonated [MX(mtbhp)] and protonated forms [MX(Hmtbhp)](ClO_4) (M = Pd^{2+}, Pt^{2+}; X = Cl^-, Br^-; Hmtbhp = 2-(2-(2-(methylthio)benzylidene)hydrazinyl)pyridine) and hydrogen-bonded proton-transfer (HBPT) assemblies containing [PdBr(mtbhp)] and bromanilic acid (H_2BA). The mtbhp hydrazone ligand acts as a tridentate SNN ligand and provides a high proton affinity. UV−vis spectroscopy revealed that these metal−hydrazone complexes follow a reversible protonation−deprotonation reaction ([MX(mtbhp)] + H^+ ⇌ [MX(Hmtbhp)]$^+$), resulting in a remarkable color change from red to yellow. Reactions between proton acceptor [PdBr(mtbhp)] (A) and proton donor H_2BA (D) afforded four types of HBPT assemblies with different D/A ratios: for D/A = 1:1, {[PdBr(Hmtbhp)](HBA)·Acetone} and {[PdBr(Hmtbhp)](HBA)·2(1,4-dioxane)}; for D/A = 1:2, [PdBr(Hmtbhp)]$_2$(BA); and for D/A = 3:2, {[PdBr(Hmtbhp)]$_2$(HBA)$_2$(H_2BA)·2Acetonitrile}. The proton donor gave at least one proton to the acceptor to form the hydrogen bonded A···D pair of [PdBr(Hmtbhp)]$^+$···HBA^-. The strength of the hydrogen bond in the pair depends on the kind of molecule bound to the free monoanionic bromanilate OH group. Low-temperature IR spectra (T < 150 K) showed that the hydrogen bond distance between [PdBr(Hmtbhp)]$^+$ and bromanilate was short enough (*ca*. 2.58 Å) to induce proton migration in the [PdBr(Hmtbhp)]$_2$(BA) assembly in the solid state. The hydrogen bonds formed not only between [PdBr(Hmtbhp)]$^+$ and HBA^- but also between HBA^- and neutral H_2BA molecules in the {[PdBr(Hmtbhp)]$_2$(HBA)$_2$(H_2BA)·2Acetonitrile} assembly. The H_2BA-based flexible hydrogen bond network and strong acidic host structure result in an interesting vapor adsorption ability and vapochromic behavior in this assembly because the vapor-induced rearrangement of the hydrogen bond network, accompanied by changes in $\pi-\pi$ stacking interactions, provides a recognition ability of proton donating and accepting properties of the vapor molecule.

1. Introduction

The design and synthesis of stable and reversible chemical sensors have received considerable attention in the past decade.[1] In particular, vapochromic materials showing pronounced and reversible changes in color and/or emission in the presence of volatile organic compounds have become increasingly attractive for their potential chemical sensing applications.[2−12] Mann and co-workers investigated the [Pt(aryl-isonitrile)$_4$][Pd(CN)$_4$] complex and suggested that the intermolecular metallophilic interaction between d^8 metal ions plays a critical role in its vapochromic behavior.[2] Taking advantage of this intermolecular metallophilic interaction, many researchers have focused on developing new vapochromic materials applicable to chemical sensors[2−7] and found that the vapochromic behavior of these materials usually originates from the structural change induced by the adsorption of vapor molecules.[3] The adsorption of vapor molecules changes intermolecular metallophilic and/or $\pi-\pi$ interactions, resulting in the perturbation of the transition energy in the visible region. Similarly, vapochromic materials using metallophilic interactions

† Department of Chemistry, Hokkaido University.
‡ Aichi University of Education.
§ Research Institute for Electronic Science, Hokkaido University.

(1) (a) De Silva, A. P.; Fox, D. B.; Huxley, A. J. M.; Moody, T. S. *Coord. Chem. Rev.* **2000**, *205*, 41–57. (b) Prodi, L.; Bolletta, F.; Montalti, M.; Zaccheroni, N. *Coord. Chem. Rev.* **2000**, *205*, 59–83. (c) Fabbrizzi, L.; Licchelli, M.; Rabaioli, G.; Taglietti, A. *Coord. Chem. Rev.* **2000**, *205*, 85–108. (d) Parker, D. *Coord. Chem. Rev.* **2000**, *205*, 109–130. (e) Beer, P. D.; Cadman, J. *Coord. Chem. Rev.* **2000**, *205*, 131–155. (f) Robertson, A.; Shinkai, S. *Coord. Chem. Rev.* **2000**, *205*, 157–199. (g) Keefe, M. H.; Benkstein, K. D.; Hupp, J. T. *Coord. Chem. Rev.* **2000**, *205*, 201–228. (h) Demas, J. N.; DeGraff, B. A. *Coord. Chem. Rev.* **2001**, *211*, 317–351. (i) Sun, S.-S.; Lees, A. J. *Coord. Chem. Rev.* **2002**, *230*, 170–191.

(2) (a) Exstrom, C. L.; Sowa, J. R., Jr.; Daws, C. A.; Janzen, D.; Mann, K. R.; Moore, G. A.; Stewart, F. F. *Chem. Mater.* **1995**, *7*, 15–17. (b) Daws, C. A.; Exstrom, C. L.; Sowa, J. R., Jr.; Mann, K. R. *Chem. Mater.* **1997**, *9*, 363–368. (c) Buss, C. E.; Anderson, C. E.; Pomije, M. K.; Lutz, C. M.; Britton, D.; Mann, K. R. *J. Am. Chem. Soc.* **1998**, *120*, 7783–7790. (d) Kunugi, Y.; Mann, K. R.; Miller, L. L.; Exstrom, C. L. *J. Am. Chem. Soc.* **1998**, *120*, 589–590.

 10.1021/ja1063444

with Au(I) ions have been also reported.[4] In addition to vapochromism, some of the Au(I) complexes also showed mechanochromism, the reversible color change induced by applying mechanical pressure. Despite extensive studies on vapochromic materials, it is still difficult to achieve vapor selectivity and recognition capability in vapochromic materials based on metallophilic interactions. This may be due to the fact that most vapochromic complexes are molecule-based assembled materials in which systematic control of the crystal structure is difficult because of nondirectional intermolecular interactions, such as van der Waals and Coulomb interactions. Much effort has been devoted to achieving vapor selectivity and recognition capability. Castellano and co-workers reported a Pt(II)-diimine based sensor microarray in which the vapor recognition capability was achieved by combining eighteen different vapochromic Pt(II)-terpyridyl chloride complexes.[7] Another approach is to incorporate well-known photofunctional molecules into solid state materials.[8] For example, fluorescent metal−organic frameworks built from photofunctional ligands and various metal ions are promising because their rigidity and permanent porosity enable shape and size selective sensing.[8] In fact, this type of materials shows guest-dependent luminescent properties.

The hydrogen bond is one of the most effective interactions for controlling crystal structure. It has been extensively utilized in various fields such as supramolecular chemistry, molecular recognition, and sensing.[9] Eisenberg and co-workers have reported the vapochromism of hydrogen bonded Pt(II)−diimine complex $[Pt(Nttpy)Cl](PF_6)_2$ (Nttpy = 4′-(*p*-nicotinamide-*N*-methylphenyl)-2,2′:6′,2″-terpyridine).[10] Naota and co-workers recently studied vapochromic organic S-shaped supramolecules in which the hydrogen bond plays an important role in both their recognition and vapor adsorption abilities.[11] We have also designed a hydrogen bonded vapochromic Pt(II) complex, $[Pt(CN)_2(H_2dcbpy)]\cdot 2H_2O$ (H_2dcbpy = 4,4′-dicarboxy-2,2′-bipyridine), and found that its vapochromism derives from the formation/deformation and transformation of the hydrogen bond network accompanied by significant changes in metallophilic interactions.[12] These studies suggest that hydrogen bonding interactions are also useful for regulating the crystal structures of vapochromic materials and may be promising for achieving vapor selectivity and recognition capability.

Our recent attention has focused on proton transfer in hydrogen bonds because proton transfer would significantly affect both proton donating and accepting molecules. The proton is known to move in the hydrogen bond when the donor−acceptor distance is sufficiently short.[13] In some cases, this proton movement can provide interesting properties such as molecular ferroelectricity.[14] In this work, aiming at constructing a new vapochromic system utilizing flexible hydrogen bonds and proton transfer, we have designed a series of hydrogen-bonded proton-transfer (HBPT) assemblies that consist of a metal−hydrazone unit as a proton acceptor and bromanilic acid as a proton donor. In this paper, we report the structures and acid−base behaviors of newly synthesized metal−hydrazone complexes [MX(mtbhp)] ($M = Pd^{2+}$, $X = Cl^-$ (**1**); $M = Pd^{2+}$, $X = Br^-$ (**2**); $M = Pt^{2+}$, $X = Cl^-$ (**3**); Hmtbhp =2-(2-(2-(methylthio)benzylidene)hydrazinyl)pyridine) and the physical properties of their HBPT

(3) (a) Kunugi, Y.; Miller, L. L.; Mann, K. R.; Pomije, M. K. *Chem. Mater.* **1998**, *10*, 1487–1489. (b) Lu, W.; Chan, M. C. W.; Cheung, K.-K.; Che, C.-M. *Organometallics* **2001**, *20*, 2477–2486. (c) Drew, S. M.; Janzen, D. E.; Buss, C. E.; MacEwan, D. I.; Dublin, K. M.; Mann, K. R. *J. Am. Chem. Soc.* **2001**, *123*, 8414–8415. (d) Buss, C. E.; Mann, K. R. *J. Am. Chem. Soc.* **2002**, *124*, 1031–1039. (e) Kato, M.; Omura, A.; Toshikawa, A.; Kishi, S.; Sugimoto, Y. *Angew. Chem.* **2002**, *114*, 3315–3317; *Angew. Chem., Int. Ed.* **2002**, *41*, 3183−3185. (f) Kishi, S.; Kato, M. *Mol. Cryst. Liq. Cryst.* **2002**, *379*, 303–308. (g) Lu, W.; Chan, M. C. W.; Zhu, N.; Che, C.-M.; He, Z.; Wong, K.-Y. *Chem.−Eur. J.* **2003**, *9*, 6155–6166. (h) Grove, L. J.; Rennekamp, J. M.; Jude, H.; Connick, W. B. *J. Am. Chem. Soc.* **2004**, *126*, 1594–1595. (i) Kui, S. C. F.; Chui, S. S.-Y.; Che, C.-M.; Zhu, N. *J. Am. Chem. Soc.* **2006**, *128*, 8297–8309. (j) Kato, M. *Bull. Chem. Soc. Jpn.* **2007**, *80*, 287–294. (k) Du, P.; Schneider, J.; Brennessel, W. W.; Eisenberg, R. *Inorg. Chem.* **2008**, *47*, 69–77. (l) Grove, L. J.; Oliver, A. G.; Krause, J. A.; Connick, W. B. *Inorg. Chem.* **2008**, *47*, 1408–1410. (m) Fornies, J.; Fuertes, S.; Lopez, J. A.; Martin, A.; Sicilia, V. *Inorg. Chem.* **2008**, *47*, 7166–7176. (n) Kobayashi, A.; Fukuzawa, Y.; Noro, S.; Nakamura, T.; Kato, M. *Chem. Lett.* **2009**, *38*, 998–999. (o) Ni, J.; Wu, Y.-H.; Zhang, X.; Li, B.; Zhang, L.-Y.; Chen, Z.-N. *Inorg. Chem.* **2009**, *48*, 10202–10210. (p) Kobayashi, A.; Hara, H.; Noro, S.; Kato, M. *Dalton Trans.* **2010**, *39*, 3400–3406. (q) Kobayashi, A.; Yonemura, T.; Kato., K. *Eur. J. Inorg. Chem.* **2010**, 2465–2470.

(4) (a) Mansour, M. A.; Connick, W. B.; Lachicotte, R. J.; Gysling, H. J.; Eisenberg, R. *J. Am. Chem. Soc.* **1998**, *120*, 1329–1330. (b) Rawashdeh-Omary, M. A.; Omary, M. A.; Fackler, J. P., Jr.; Galassi, R.; Pietroni, B. R.; Burini, A. *J. Am. Chem. Soc.* **2001**, *123*, 9689–9691. (c) Fernández, E. J.; López-de-Luzuriaga, J. M.; Monge, M.; Olmos, M. E.; Pérez, J.; Laguna, A.; Mohamed, A. A.; Fackler, J. P., Jr. *J. Am. Chem. Soc.* **2003**, *125*, 2022–2023. (d) Fernández, E. J.; López-de-Luzuriaga, J. M.; Monge, M.; Montiel, M.; Olmos, M. E.; Pérez, J.; Laguna, A.; Mendizabal, F.; Mohamed, A. A.; Fackler, J. P., Jr. *Inorg. Chem.* **2004**, *43*, 3573–3581. (e) Lefebvre, J.; Batchelor, R. J.; Leznoff, D. B. *J. Am. Chem. Soc.* **2004**, *126*, 16117–16125.

(5) (a) Ir: Liu, Z.; Bian, Z.; Bian, J.; Li, Z.; Nie, D.; Huang, C. *Inorg. Chem.* **2008**, *47*, 8025–8030. (b) Ru: McGee, K. A.; Marquardt, B. J.; Mann, K. R. *Inorg. Chem.* **2008**, *47*, 9143–9145.

(6) (a) Co: Beauvais, L. G.; Shores, M. P.; Long, J. R. *J. Am. Chem. Soc.* **2000**, *122*, 2763–2772. (b) Cu: Yamada, K.; Yagishita, S.; Tanaka, H.; Tohyama, K.; Adachi, K.; Kaizaki, S.; Kumagai, H.; Inoue, K.; Kitaura, R.; Chang, H.-C.; Kitagawa, S.; Kawata, S. *Chem.−Eur. J.* **2004**, *10*, 2647–2660. (c) Yamada, K.; Tanaka, H.; Yagishita, S.; Adachi, K.; Uemura, T.; Kitagawa, S.; Kawata, S. *Inorg. Chem.* **2006**, *45*, 4322–4324. (d) Ag: Fernández, E. J.; López-de-Luzuriaga, J. M.; Monge, M.; Olmos, M. E.; Puelles, R. C.; Laguna, A.; Mohamed, A. A.; Fackler, J. P., Jr. *Inorg. Chem.* **2008**, *47*, 8069–8076.

(7) Muro, M. L.; Daws, C. A.; Castellano, F. N. *Chem. Commun.* **2008**, 6134–6136.

(8) (a) Chen, B.; Wang, L.; Zapata, F.; Qian, G.; Lobkovsky, E. B. *J. Am. Chem. Soc.* **2008**, *130*, 6718–6719. (b) Allendorf, M. D.; Bauer, C. A.; Bhakta, R. K.; Houk, R. J. T. *Chem. Soc. Rev.* **2009**, *38*, 1330–1352. (c) Stylianou, K. C.; Heck, R.; Chong, S. Y.; Bacsa, J.; Jones, J. T. A.; Khimyak, Y. Z.; Bradshaw, D.; Rosseinsky, M. J. *J. Am. Chem. Soc.* **2010**, *132*, 4119–4130.

(9) (a) MacDonald, J. C.; Whitesides, G. M. *Chem. Rev.* **1994**, *94*, 2363–2420. (b) Zaman, M. B.; Tomura, M.; Yamashita, Y. *J. Org. Chem.* **2001**, *66*, 5987–5995. (c) Sobczyk, L.; Grabowski, S. J.; Krygowski, T. M. *Chem. Rev.* **2005**, *105*, 3513–3560. (d) Lena, S.; Masiero, S.; Pieraccini, S.; Spada, G. P. *Chem.−Eur. J.* **2009**, *16*, 7792–7806. (e) Boldog, I.; Daran, J.-C.; Chernega, A. N.; Rusanov, E. B.; Krautscheid, H.; Domasevitch, K. V. *Cryst. Growth Des.* **2009**, *9*, 2895–2905.

(10) Wadas, T. J.; Wang, Q.-M.; Kim, Y.-J.; Flaschenreim, C.; Blanton, T. N.; Eisenberg, R. *J. Am. Chem. Soc.* **2004**, *126*, 16841–16849.

(11) Takahashi, E.; Takaya, H.; Naota, T. *Chem.−Eur. J.* **2010**, *16*, 4793–4802.

(12) Kato, M.; Kishi, S.; Wakamatsu, Y.; Sugi, Y.; Osamura, Y.; Koshiyama, T.; Hasegawa, M. *Chem. Lett.* **2005**, *34*, 1368–1369.

(13) (a) Ishida, H.; Kashino, S. *Acta Crystallogr., Sect. C* **1999**, *55*, 1714–1717. (b) Nihei, T.; Ishimaru, S.; Ishida, H.; Ishihara, H.; Ikeda, R. *Chem. Lett.* **2000**, 1346–1347. (c) Ikeda, R.; Takahashi, S.; Nihei, T.; Ishihara, H.; Ishida, H. *Bull. Chem. Soc. Jpn.* **2005**, *78*, 1241–1245. (d) Sawka-Dobrowolska, W.; Bator, G.; Sobczyk, L.; Grech, E.; Nowicka-Scheibe, J.; Pawlukojc, A. *Struct. Chem.* **2005**, *16*, 281–286. (e) Suzuki, H.; Mori, H.; Yamaura, J.; Matsuda, M.; Tajima, H.; Mochida, T. *Chem. Lett.* **2007**, *36*, 402–403.

(14) (a) Szafranski, M.; Katrusiak, A.; McIntyre, G. *Phys. Rev. Lett.* **2002**, *89*, 215507. (b) Horiuchi, S.; Ishii, F.; Kumai, R.; Okimoto, Y.; Tachibana, H.; Nagaosa, N.; Tokura, Y. *Nat. Mater.* **2005**, *4*, 163–166. (c) Kumai, R.; Horiuchi, S.; Okimoto, Y.; Tokura, Y. *J. Chem. Phys.* **2006**, *125*, 084715. (d) Horiuchi, S.; Kumai, R.; Tokura, Y. *Angew. Chem., Int. Ed.* **2007**, *46*, 3497–3501. (e) Horiuchi, S.; Kumai, R.; Tokunaga, Y.; Tokura, Y. *J. Am. Chem. Soc.* **2008**, *130*, 13382–13391. (f) Horiuchi, S.; Tokunaga, Y.; Giovannetti, G.; Picozzi, S.; Itoh, H.; Shimano, R.; Kumai, R.; Tokura, Y. *Nature* **2010**, *463*, 789–792.

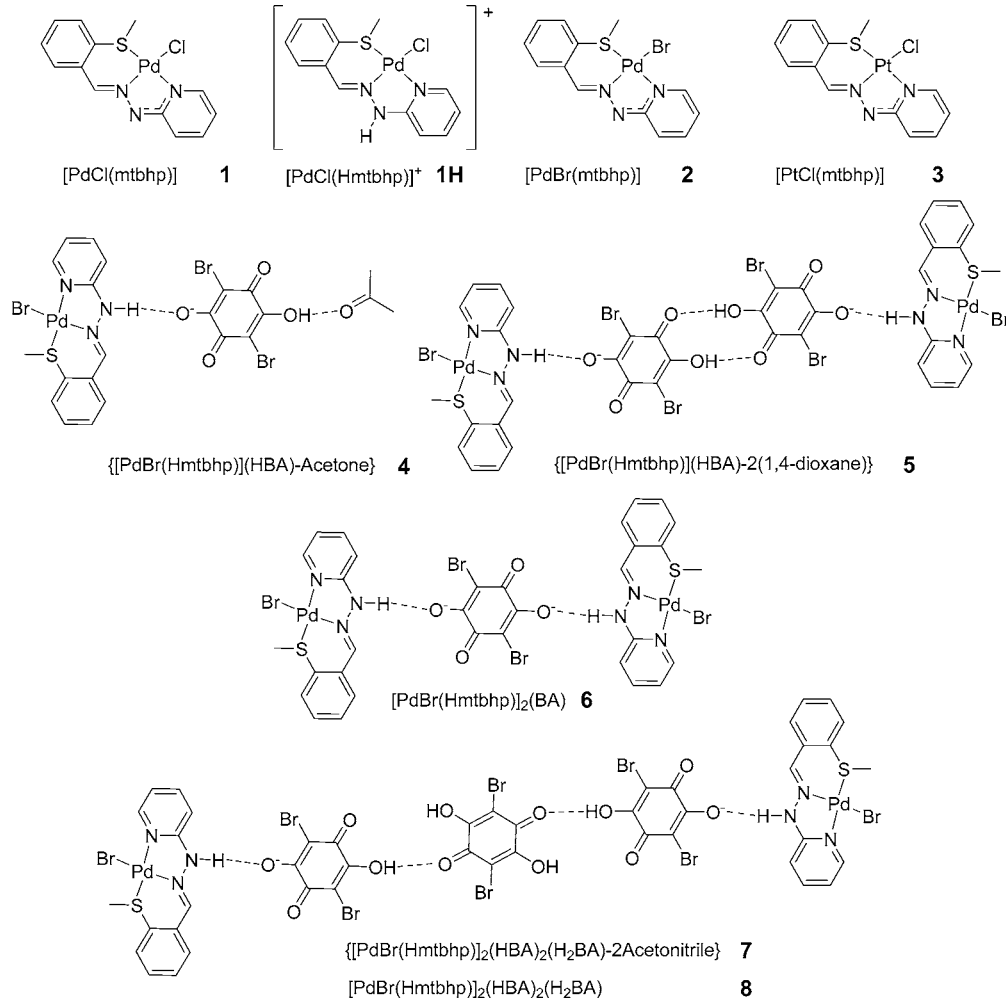

Figure 1. Structural representation of metal−hydrazone complexes **1**−**3** and **1H** and their proton transfer assemblies **4**−**8**.

assemblies {[PdBr(Hmtbhp)](HBA)·Acetone} (**4**), {[PdBr(Hmtbhp)](HBA)·2(1,4-dioxane)} (**5**), [PdBr(Hmtbhp)]$_2$(BA) (**6**), and {[PdBr(Hmtbhp)]$_2$(HBA)$_2$(H$_2$BA)·2CH$_3$CN} (**7**) (H$_2$BA = bromanilic acid; HBA = monoanionic bromanilate) (Figure 1). We also demonstrate that HBPT assembly **7** is a new vapochromic material that can recognize the proton donating/accepting ability of the vapor. To the best of our knowledge, this is the first proton donor−acceptor based vapochromic material that does not involve metallophilic interactions.

2. Experimental Section

General Procedures. CAUTION! *Although we experienced no difficulties, perchlorate salts are potentially explosive and should only be used in small quantities and handled with care.*

All commercially available starting materials were used as received, and solvents were used without any purification. Unless otherwise stated, all manipulations were performed in air. 2-Methylthio-benzaldehyde, 2-hydrazinopyridine, PdCl$_2$, PdBr$_2$, K$_2$PtCl$_4$, and bromanilic acid (H$_2$BA) were purchased from Wako Pure Chemical Industries, Ltd. Japan. PdCl$_2$(PhCN)$_2$, PdBr$_2$(PhCN)$_2$, and PtCl$_2$(PhCN)$_2$ (PhCN = benzonitrile) were prepared according to published methods.[15]

(15) (a) Doyle, J. R.; Slade, P. E.; Jonassen, H. B. *Inorg. Synth.* **1960**, *6*, 218–219. (b) Braunstein, P.; Bender, R.; Jud, J. *Inorg. Synth.* **1989**, *26*, 341–350. (c) Anderson, G. K.; Lin, M. *Inorg. Synth.* **1990**, *28*, 61–62.

Hmtbhp. 2-Hydrazinopyridine (333.0 mg, 3.05 mmol) was added to a 2-methylthio-benzaldehyde (462.8 mg, 3.04 mmol) solution in methanol (10 mL) and refluxed for 1 h. The reaction solution was cooled to room temperature, allowing a pale-yellow precipitate to emerge gradually. The precipitate was filtered, washed using diethylether, and vacuum-dried for 1 h to afford Hmtbhp as a pale yellow crystalline powder. Yield: 558.4 mg, 75.2% (based on 2-methylthio-benzaldehyde). Elemental analysis calcd for $C_{13}H_{13}N_3S_1$: C, 64.17; H, 5.38; N, 17.27. Found: C, 64.05; H, 5.37; N, 17.21.

[PdCl(mtbhp)] (1). A solution of Hmtbhp ligand (31.7 mg, 0.13 mmol) in acetonitrile (10 mL) was added to a solution of PdCl$_2$(PhCN)$_2$ (50 mg, 0.13 mmol) in acetonitrile (10 mL) in a light resistant flask. Triethylamine (13.4 mg, 0.13 mmol) was added slowly to the reaction mixture, which was then allowed to stand for 1 d in the dark until reddish-purple platelets emerged. The crystals were isolated by filtration, washed using a small amount of acetonitrile, and then dried under vacuum. Yield: 31.3 mg, 63.5% (based on PdCl$_2$(PhCN)$_2$). Elemental analysis calcd for $C_{13}H_{12}ClN_3SPd$: C, 40.64; H, 3.15; N, 10.94. Found: C, 40.45; H, 3.11; N, 10.98.

[PdBr(mtbhp)] (2). Bromide complex **2** was obtained through a similar synthetic method as **1** but using PdBr$_2$(PhCN)$_2$ instead of PdCl$_2$(PhCN)$_2$. Yield: 43.4 mg, 77.9% (based on PdBr$_2$(PhCN)$_2$). Elemental analysis calcd for $C_{13}H_{12}BrN_3SPd$: C, 36.43; H, 2.82; N, 9.80. Found: C, 36.21; H, 2.74; N, 9.73.

[PtCl(mtbhp)] (3). A solution of Hmtbhp ligand (36.7 mg, 0.15 mmol) in acetonitrile (15 mL) was added to a solution of PtCl$_2$(PhCN)$_2$ (71.1 mg, 0.15 mmol) in acetonitrile (15 mL) in a

light resistant flask. Triethylamine (15.5 mg, 0.15 mmol) was added slowly to the reaction mixture, which was refluxed for 3 h in the dark and then allowed to cool to room temperature. The solvent was evaporated to about 5 mL to give a red crystalline precipitate. The precipitate was isolated by filtration, washed using a small amount of acetonitrile, and then dried under vacuum. Yield: 49.3 mg, 51.5% (based on $PtCl_2(PhCN)_2$). Elemental analysis calcd for $C_{13}H_{12}ClN_3SPt$: C, 33.02; H, 2.56; N, 8.89. Found: C, 33.07; H, 2.84; N, 8.87.

[PdCl(Hmtbhp)](ClO_4) (1H). Perchloric acid (10 equiv) was added to a solution of **1** (3.0 mg, 7.83 μmol) in acetonitrile. The solution color immediately changed from dark red to yellow. Diethyl ether vapors were allowed to diffuse into the solution for 3 d to afford [PdCl(Hmtbhp)](ClO_4) as pale yellow crystals. The crystals were filtered, washed using diethyl ether, and dried under vacuum for 1 h. Yield: 1.6 mg, 42% (based on **1**). Elemental analysis calcd for $C_{13}H_{13}Cl_2N_3O_4SPd$: C, 32.22; H, 2.70; N, 8.67. Found: C, 31.86; H, 2.94; N, 8.85.

{[PdBr(Hmtbhp)](HBA)·(CH_3)$_2$CO} (4). A solution of H_2BA (23.3 mg, 78.2 mmol) in acetone (10 mL) was added to a solution of **2** (3.0 mg, 7.8 mmol), in acetone (10 mL) in a light resistance flask. Reddish-purple needle crystals of **4** emerged by natural evaporation for several days. The crystals were isolated by filtration, washed with a small amount of acetonitrile, and air-dried. Yield: 3.2 mg, 53% (based on **2**). Elemental analysis calcd for $C_{22}H_{20}Br_3N_3O_5SPd$: C, 33.68; H, 2.57; N, 5.36. Found: C, 33.41; H, 2.40; N, 5.09.

{[PdBr(Hmtbhp)](HBA)·2(1,4-dioxane)} (5). A solution of H_2BA (230 mg, 772.3 mmol) in 1,4-dioxane (30 mL) was added to a solution of **2** (33.0 mg, 78.0 mmol), in 1,4-dioxane (70 mL) in a light resistance flask. Dark-red platelet crystals of **5** emerged by natural evaporation for several weeks. The crystals were isolated by filtration, washed with a small amount of 1,4-dioxane, and air-dried. Yield: 13.5 mg, 19.3% (based on **2**). Elemental analysis calcd for $C_{21}H_{18}Br_3N_3O_5SPd$: C, 32.73; H, 2.35; N, 5.45. Found: C, 32.69; H, 2.59; N, 5.26.

[PdBr(Hmtbhp)]$_2$(BA) (6). Solutions of H_2BA (2.3 mg, 7.8 mmol) and 10 equiv of pyrazine (3.1 mg, 39 mmol) in acetonitrile (10 mL) were added to a solution of **2** (3.0 mg, 7.8 mmol), in acetonitrile (30 mL) in a light resistance flask. Red platelets of **6** emerged by natural evaporation for several days. The crystals were isolated by filtration, washed using a small amount of acetonitrile, and then air-dried. Yield: 2.5 mg, 28% (based on **2**). Elemental analysis calcd for $C_{32}H_{26}Br_4N_6O_4Pd_2S_2$: C, 33.27; H, 2.27; N, 7.28. Found: C, 33.23; H, 2.15; N, 7.12.

{[PdBr(Hmtbhp)]$_2$(HBA)$_2$(H_2BA)·2CH_3CN} (7). A solution of H_2BA (23.0 mg, 77.2 mmol) in acetonitrile (10 mL) was added to a solution of **2** (3.3 mg, 7.7 mmol) in acetonitrile (10 mL) in a light resistance flask. Reddish-purple needle crystals of **7** emerged by natural evaporation for several days. The crystals were isolated by filtration, washed with a small amount of acetonitrile, and then air-dried. Yield: 3.8 mg, 54% (based on **2**). Elemental analysis calcd for $C_{24}H_{18}Br_4N_4O_6SPd$: C, 31.45; H, 1.98; N, 6.11. Found: C, 31.17; H, 2.03; N, 5.93.

Single Crystal X-ray Diffraction Measurements. All single crystal X-ray diffraction measurements were performed using a Rigaku Mercury CCD diffractometer with graphite monochromated Mo Kα radiation (λ = 0.710 69 Å) and a rotating anode generator. Each single crystal was mounted on a glass fiber with epoxy resin. The crystal temperature was cooled down using a N_2-flow type temperature controller. Diffraction data were collected and processed using the CrystalClear software.[16] Structures were solved by the direct method using SIR-2004 for **1**, **2**, **5**, **6**, and **7**; SIR-92 for **4**; and SHELXS-97 for **1H**.[17−19] Structural refinements were performed by full-matrix least-squares using SHELXL-97. Non-

Table 1. Crystal Parameters and Refinement Data

Complex	**1**	**2**	**1H**	**4**	**5**	**6**	**6**	**6**	**7**
T/K	153(1)	150(1)	150(1)	150(1)	250(1)	110(1)	150(1)	250(1)	150(1)
formula	$C_{13}H_{12}ClN_3PdS$	$C_{13}H_{12}BrN_3PdS$	$C_{13}H_{13}Cl_2N_3O_4PdS$	$C_{22}H_{20}Br_3N_3O_5PdS$	$C_{27}H_{30}Br_3N_3O_8PdS$	$C_{32}H_{26}Br_4N_6O_4Pd_2S_2$	$C_{32}H_{26}Br_4N_6O_4Pd_2S_2$	$C_{32}H_{26}Br_4N_6O_4Pd_2S_2$	$C_{24}H_{16}Br_4N_4O_6PdS$
formula weight	384.17	428.62	484.63	784.59	902.75	1155.13	1155.13	1155.13	914.49
crystal system	monoclinic	monoclinic	triclinic	monoclinic	triclinic	monoclinic	monoclinic	monoclinic	monoclinic
space group	$P2_1/c$	$P2_1/c$	$P\bar{1}$	$C2/c$	$P\bar{1}$	$C2/c$	$C2/c$	$C2/c$	$P2_1/n$
a/Å	7.297(3)	7.2466(10)	8.645(3)	32.506(5)	9.779(2)	40.443(8)	40.506(9)	40.66(2)	13.980(4)
b/Å	8.506(3)	8.6870(7)	9.574(3)	8.6406(13)	12.792(3)	8.8478(15)	8.8629(16)	8.883(4)	4.8149(13)
c/Å	21.594(8)	21.727(2)	9.938(3)	21.204(4)	13.927(3)	21.617(4)	21.647(5)	21.737(11)	42.220(12)
α/deg	90	90	86.455(8)	90	97.402(2)	90	90	90	90
β/deg	92.523(6)	92.269(5)	87.410(9)	120.6663(15)	96.785(2)	117.8615(5)	117.6530(8)	117.6190(18)	98.1321(8)
γ/deg	90	90	82.196(8)	90	110.977(3)	90	90	90	90
V/Å^3	1338.9(8)	1366.7(3)	821.8(5)	5122.8(14)	1587.5(7)	6850(2)	6884(2)	6957(6)	2813.3(13)
Z	4	4	2	8	2	8	8	8	4
D_{calcd}/ g·cm^{-3}	1.906	2.083	1.980	2.034	1.888	2.240	2.229	2.206	2.159
reflections collected	9768	10556	6612	20276	12680	25619	25699	25536	16116
unique reflections	3035	3120	3647	5856	6948	7815	7852	7903	6296
GOF	1.191	1.096	1.091	1.113	0.996	0.967	1.020	1.064	0.857
R	0.0342	0.0258	0.037	0.0267	0.0469	0.0338	0.0356	0.0437	0.0384
R_w	0.0899	0.0649	0.081	0.0591	0.1266	0.0758	0.0836	0.1079	0.0670

(16) CrystalClear: Molecular Structure Corporation, Orem, UT, 2001.
(17) SIR2004: Burla, M. C.; Caliandro, R.; Camalli, M.; Carrozzini, B.; Cascarano, G. L.; De Caro, L.; Giacovazzo, C.; Polidori, G.; Spagana, R. *J. Appl. Crystallogr.* **2005**, *38*, 381–388.

Table 2. Selected Bond Lengths and Angles of the Hydrazone Ligand for Metal−Hydrazone Complexes **1**, **2**, and **1H** and HBPT Assemblies **4**, **5**, **6**, and **7**

						6 at 110 K		**6** at 150 K		**6** at 250 K		
	1	**2**	**1H**	**4**	**5**	(*S*)	(*R*)[a]	(*S*)	(*R*)[a]	(*S*)	(*R*)[a]	**7**
C6−C7	1.450(4)	1.448(3)	1.450(4)	1.450(5)	1.459(8)	1.464(5)	1.464(5)	1.460(5)	1.463(5)	1.443(5)	1.454(6)	1.463(7)
C7−N1	1.301(4)	1.304(3)	1.273(4)	1.291(4)	1.261(8)	1.283(6)	1.285(7)	1.293(6)	1.288(6)	1.310(7)	1.289(7)	1.279(6)
N1−N2	1.382(3)	1.375(2)	1.374(4)	1.378(4)	1.377(6)	1.378(4)	1.387(4)	1.380(4)	1.378(4)	1.366(4)	1.374(4)	1.394(6)
N2−C8	1.337(4)	1.342(3)	1.369(4)	1.360(4)	1.376(9)	1.357(7)	1.350(7)	1.352(6)	1.361(6)	1.370(7)	1.368(7)	1.351(6)
C8−N3	1.369(4)	1.372(2)	1.343(4)	1.346(2)	1.330(7)	1.344(6)	1.351(6)	1.348(6)	1.347(6)	1.341(7)	1.341(6)	1.355(7)
C8−C9	1.420(4)	1.423(3)	1.394(5)	1.396(4)	1.389(8)	1.404(5)	1.402(5)	1.402(5)	1.410(5)	1.392(6)	1.412(6)	1.387(8)
N2−H13	−	−	0.82(4)	0.82(2)	0.85(6)	1.34(7)	−	1.22(7)	−	1.11(7)	−	0.88(4)
N2b−H13b	−	−	−	−	−	−	1.61(8)	−	1.24(8)	−	1.11(6)	−
N1−N2−C8	111.8(2)	112.3(2)	119.2(3)	118.3(2)	119.6(5)	117.4(4)	117.7(3)	118.2(3)	117.4(3)	117.4(4)	117.8(4)	119.0(4)

[a] (*R*)-[PdBr(Hmtbhp)]$^+$ unit in **6** was labeled with an additional character "b".

Table 3. Selected Bond Lengths of the Bromanilate Anion in HBPT Assemblies **4**, **5**, **6**, and **7**

			6			
	4	**5**	110 K	150 K	250 K	**7**
C15−O1	1.327(2)	1.343(7)	1.275(7)	1.272(6)	1.276(7)	1.321(6)
C16−O2	1.239(3)	1.229(6)	1.224(6)	1.229(6)	1.237(7)	1.246(6)
C18−O3	1.256(2)	1.239(9)	1.274(7)	1.280(6)	1.281(7)	1.227(6)
C19−O4	1.215(3)	1.212(7)	1.227(7)	1.225(6)	1.228(7)	1.210(6)

Table 4. Hydrogen Bond (NH···O) Distances between [PdBr(Hmtbhp)]$^+$ and HBA$^-$ in HBPT Assemblies **4**, **5**, **6**, and **7**

			6			
	4	**5**	110 K	150 K	250 K	**7**
N2−H13···O3	2.653(2)	2.597(8)	2.585(6)	2.584(5)	2.577(6)	2.679(5)
N2b−H13b···O1	−	−	2.580(5)	2.588(5)	2.594(6)	−

hydrogen atoms were refined anisotropically, hydrogen atoms bound to nitrogen or oxygen atoms were refined isotropically, and other hydrogen atoms were refined using the riding model. All calculations were performed using the Crystal Structure crystallographic software package.[20] Crystallographic data obtained for each complex are summarized in Table 1. Selected bond lengths and angles are shown in Tables 2 and 3 for metal−hydrazone and bromanilate units, respectively. Hydrogen bond distances are reported in Table 4.

Powder X-ray Diffraction. Powder X-ray diffraction measurement was performed using a Rigaku SPD diffractometer at beamline BL-8B, Photon Factory, KEK, Japan. The wavelength of the synchrotron X-ray was 1.200(1) Å. Every sample was placed in a glass capillary of 0.5 mmϕ diameter.

UV−vis Spectroscopy. The UV−vis adsorption spectrum of each complex was recorded on a Shimadzu UV-2400PC spectrophotometer. The diffuse reflectance spectrum of each complex was recorded on the same spectrophotometer equipped with an integrating sphere apparatus. Obtained reflectance spectra were converted to absorption spectra using the Kubelka−Munk function $F(R_\infty)$.

IR Spectroscopy. For IR absorption measurements, samples were prepared by grinding single crystals with KBr and processing the mixtures into pellets using a press (∼6 kbar) under vacuum. Temperature dependent IR spectra were recorded on a Thermo-Nicolet 6700 FT-IR spectrometer. The sample temperature was controlled using an Oxford MicrostatHe instrument.

(18) SIR92: Altomare, A.; Cascarano, G.; Giacovazzo, C.; Guagliardi, A.; Burla, M.; Polidori, G.; Camalli, M. *J. Appl. Crystallogr.* **1994**, *27*, 435–436.
(19) SHELX97: Sheldrick, G. M. *Acta Crystallogr., Sect. A* **2008**, *64*, 112–122.
(20) CrystalStructure 3.7.0: Crystal Structure Analysis Package, Rigaku and Rigaku/MSC (2000−2005).

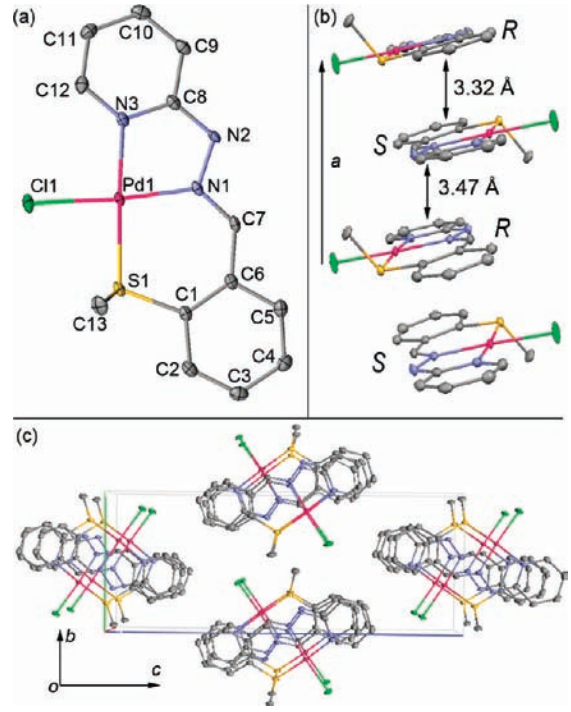

Figure 2. (a) Molecular structure of **1**, (b) alternate $\pi-\pi$ stacking of *R*- and *S*-isomers along the *a* axis, and (c) packing diagram of **1** in the *bc* plane with thermal vibrational ellipsoids at the 50% probability level. Hydrogen atoms are omitted for clarity.

Thermogravimetric Analysis. Thermogravimetry and differential thermal analysis were performed using a Rigaku ThermoEvo TG8120 analyzer.

Adsorption Isotherms. Adsorption isotherms of organic solvent vapors were measured using an automatic volumetric adsorption apparatus (BELSORP-MAX and BELSORP-mini; BEL Japan, Inc.). Before each measurement, the sample was dried at 373 K under vacuum.

3. Results and Discussion

3.1. Crystal Structures of Metal−Hydrazone Complexes. First, we studied the effect of protonation on molecular and crystal structures. Metal−hydrazone complexes **1**−**3** showed a reversible protonation−deprotonation reaction in solution (see below), and we succeeded in isolating both deprotonated [PdCl(mtbhp)] (**1**) and protonated [PdCl(Hmtbhp)](ClO$_4$) (**1H**) forms as single crystals.

3.1.1. Deprotonated Form [PdX(mtbhp)] (X = Cl, Br). Figure 2a shows the molecular structure of **1**. The deprotonated form **1** crystallizes in the monoclinic $P2_1/c$ space group. The tridentate

mtbhp ligand is coordinated to Pd^{2+} ions through two pyridyl and hydrazone N atoms and the methyl-thio S atom. All atoms are located on the same plane except for the methyl group. Owing to the chirality of the mtbhp ligand S atom, the [PdCl(mtbhp)] molecule adopts a spiral configuration to produce two (*R*)-[PdCl(mtbhp)] and (*S*)-[PdCl(mtbhp)] chiral molecules. As shown in Figure 2b, these two enantiomers are alternately stacked and form one-dimensional (1-D) columns along the *a* axis, resulting in the formation of the racemic crystal (*R,S*)-[PdCl(mtbhp)]. Within the 1-D columns, the long distance between Pd ions (Pd···Pd > 4.9 Å) indicates no metallophilic interactions. Because of the steric effect of the methyl group, the [PdCl(mtbhp)] units are weakly dimerized through relatively strong $\pi-\pi$ interactions, consistent with the 3.32 Å distance between two [PdCl(mtbhp)] molecular planes. In dimers formed by pairs of (*R*)- and (*S*)-isomers, two [PdCl(mtbhp)] molecular planes overlap and the methyl groups of the mtbhp ligands are directed to the outside of the dimer. As a result, the $\pi-\pi$ interactions are stronger in the dimer than between dimers (3.47 Å). The bromide complex [PdBr(mtbhp)] (**2**) obtained by ligand substitution has an isomorphic structure of **1**, as shown by its same space group of $P2_1/c$. The bond distances in the mtbhp ligand of **1** and **2** are almost the same (Table 2), suggesting that substitution of the chloride ion by a bromide ion hardly affects the molecular structure of the metal−hydrazone complex. However, the distances between [PdBr(mtbhp)] molecular planes were slightly shorter within the 1-D column of **2** (3.31 and 3.45 Å) than in that of **1** (3.32 and 3.47 Å). This difference may be due to the steric effect of the larger bromide ions, which causes each molecule to slightly slip toward opposite directions relative to each other in the *bc* plane to reduce the steric effect. As a result, the absorption band observed around 600 nm in the diffuse reflectance spectrum of **2** slightly shifted by about 20 nm to longer wavelengths compared to that of **1**, consistent with the shorter $\pi-\pi$ stacking distances (see Figure S1 in the Supporting Information).

3.1.2. Protonated Form [PdCl(mtbhp)](ClO_4) (1H). The molecular framework and the chirality of **1H** are almost the same as those for **1**. In particular, the bond lengths and angles of the methyl-thio-benzene ring are almost the same as those in **1H** and **1**. However, protonation of the hydrazone N2 atom significantly affected the bond lengths around hydrazone and pyridine groups. As shown in Table 2, the N2−C8 bond lengthened by about 0.03 Å, while C7−N1, C8−N3, and C8−C9 bonds shortened by about 0.03 Å upon protonation. The N1−N2−C8 bond angle (119.2(3)°) also increased by about 7° to almost reach 120°, which is an ideal bond angle of sp^2 hybridized atoms. Bond lengths around the pyridine ring of **1H** are therefore very close to typical values for pyridine and related substances.[21] These differences suggest that protonation of the hydrazone N2 atom affects the degree of the π electron delocalization in the mtbhp ligand. In other words, the pyridine π electrons are delocalized not only in the ring but also in the hydrazone of **1**, whereas the delocalization is limited to the pyridine ring upon protonation of the hydrazone moiety. The $[PdCl(Hmtbhp)]^+$ cations are hydrogen-bonded to the ClO_4^- counteranions (2.838(4) Å). Similar to the case for **1**, both (*R*)- and (*S*)-$[PdCl(Hmtbhp)]^+$ units are stacked alternately along the *b* axis in **1H** (Figure 3). Compared with deprotonated form **1**, the distance between two adjacent $[PdCl(Hmtbhp)]^+$ molecular planes (3.40 Å) increased by about 0.09 Å in **1H**, suggesting that $\pi-\pi$ interactions are weaker in **1H** than in **1**. This may be due to either Coulomb repulsion between the $[PdCl(Hmtbhp)]^+$ cations or steric hindrance of the perchlorate anion.

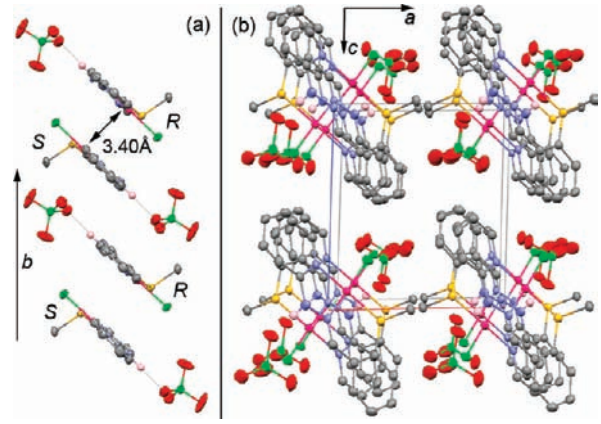

Figure 3. (a) Stacking structure and (b) packing diagram of **1H** along the *b* axis with thermal vibrational ellipsoids at the 50% probability level. Dotted lines show hydrogen bonds. Carbon-bound hydrogen atoms are omitted for clarity.

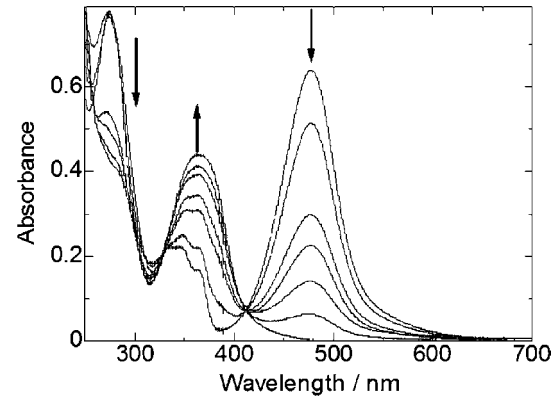

Figure 4. Changes in the absorption of **1** in acetonitrile upon addition of 70% aq. $HClO_4$. Spectra were acquired for 0, 0.25, 0.5, 0.60, 0.70, 0.80, 1.00, and 1.20 equiv additions of acid.

3.2. Protonation and Deprotonation Reactions of Metal−Hydrazone Complexes. Strong bases are known to remove a proton that binds to the hydrazone group, indicating that the acid dissociation constant (pK_a) of hydrazones is not so low.[22] In fact, the proton bound to the Hmtbhp ligand N2 atom could not be removed until the pH reached 10.4 (see Figure S2), suggesting that the pK_a value of the Hmtbhp ligand is higher than 10.4. The proton affinity of the metal−hydrazone complex was examined through acidic and basic titrations in solution. The reactions were monitored by UV−vis absorption spectroscopy. Figure 4 shows the UV−vis absorption spectral changes of **1** upon addition of perchloric acid in acetonitrile. The absorption maximum (λ_{max}), molar absorption coefficient (ε), and acid-dissociation constant (pK_a) are given in Table 5 for **1**, [PdBr(mtbhp)] (**2**), and [PtCl(mtbhp)] (**3**). Before the addition of $HClO_4$, an absorption band attributable to the intraligand charge transfer (ILCT) transition in the hydrazone ligand was observed at 474 nm.[22] The ILCT band decreased and a new

(21) (a) Siedle, A. R.; Pignolet, L. H. *Inorg. Chem.* **1982**, *21*, 135–141. (b) Tebbe, K.-F.; Grafe-Kavoosian, A.; Freckmann, B. *Z. Naturforsch., B: Chem. Sci.* **1996**, *51*, 999–1007.

(22) (a) Kohata, K.; Kawamonzen, Y.; Odashima, T.; Ishii, H. *Bull. Chem. Soc. Jpn.* **1990**, *63*, 3398–3404. (b) Lub, Y.-H.; Lua, Y.-W.; Wu, C.-L.; Shao, Q.; Chen, X.-L.; Bimbong, R. N. B. *Spectrochim. Acta A* **2006**, *65*, 695–701.

Table 5. Electronic Transition Data and Acid Dissociation Constants of [MX(mthbhp)] Complexes

Complex	λ_{max}/nm	ε/M^{-1}cm^{-1}	pK_a[a]
1	474	1.78×10^4	3.6
2	477	2.45×10^4	3.6
3	490	2.50×10^4	3.4

[a] Measured in 1:1 CH_3CN/H_2O.

absorption band appeared at 365 nm upon acid addition, while the isosbectic points were maintained at 327 and 411 nm. Conversely, the original spectrum of **1** was recovered upon addition of a base like triethylamine. These changes clearly show that the protonation of **1** and deprotonation of **1H** occur without any decomposition. The pK_a value of **1** was determined to be 3.6 in a 1:1 acetonitrile/water mixture using the pH-dependent absorbance at 477 nm (see Figure S3). [PdBr(mtbhp)] (**2**) and [PtCl(mtbhp)] complexes (**3**) also exhibited reversible protonation/deprotonation reaction upon acid or base addition (see Figure S3). The ILCT band wavelengths of **2** and **3** were found to be 477 and 490 nm, respectively. The pK_a value of **2** was the same as that of **1**, while that of **3** was found to be slightly smaller. The differences between the three [MX(mtbhp)] complexes indicate that, unlike the halide ligand substitution, the substitution of the metal ions affects the electronic property of these complexes. This result may originate from the difference in electronegativity between Pt and Pd atoms (2.28 and 2.20, respectively). Compared to other metal−hydrazone complexes, such as [CuI(Hpbph)] or [PtCl(pbph)] (Hpbph = 2-(diphenylphosphino)benzaldehyde-2-pyridylhydrazone),[23] these complexes have relatively small pK_a values. The reasons for these strong acid properties may be the high planarity of the hydrazone ligand and/or electron donating ability of the methyl-thio group. We have previously reported that the high planarity contributes to the stabilization of the deprotonated form in which π-electrons are delocalized in the entire ligand.[23]

3.3. Crystal Structures of Hydrogen-Bonded Proton-Transfer Assemblies. Because of its ability to accept one electron and donate two protons, H_2BA has been widely used to construct hydrogen bonded supramolecular architectures and molecular ferroelectric materials.[13,14] To investigate the hydrogen bonding and proton-transfer property of the [MX(mtbhp)] complexes, we synthesized new HBPT assemblies using the metal−hydrazone complex and H_2BA. In this section, we discuss the molecular and crystal structures of these assemblies from the view points of proton transfer and hydrogen bonding.

3.3.1. 1:1 Assembly between [PdBr(mtbhp)] and H_2BA. The reaction between deprotonated form **2** and H_2BA in acetone afforded the 1:1 adduct {[PdBr(Hmtbhp)](HBA)·Acetone} (**4**) as a crystalline material. Figure 5a shows the three-component hydrogen bond network between the Pd complex, bromanilic acid, and acetone for **4**. The HBPT assembly (**4**) crystallizes in the monoclinic *C*2/*c* space group. The bond lengths and angles of the hydrazone ligand are very close to those of protonated complex **1H** (Table 2), indicating that the [PdBr(mtbhp)] molecule accepts one proton from the bromanilic acid to form a proton donor−acceptor (D···A) pair. Table 3 also shows three shorter C═O and one longer C−O bond lengths for bromanilic acid, consistent with typical values for monoanionic bromanilate

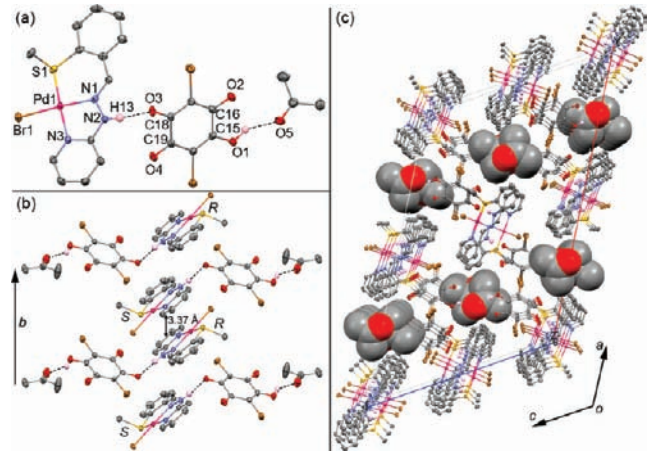

Figure 5. (a) A-D-S type hydrogen bond network, (b) stacking structure, and (c) packing diagram of **4** along the *b* axis with thermal vibrational ellipsoids at the 50% probability level. Acetone molecules are shown as space filling models. Dotted lines represent hydrogen bonds. Carbon-bound hydrogen atoms are omitted for clarity.

(HBA$^-$).[24] The remaining monoanionic bromanilate OH group is hydrogen-bonded to the acetone solvent molecule (O−H···O = 2.796 Å), leading to an A···D···S (S: solvent) type hydrogen-bonded network. The NH···O hydrogen bond distance between [PdBr(Hmtbhp)]$^+$ and HBA$^-$ is 2.653 Å, which is shorter than the typical value (*ca.* 2.89 Å).[25] The three components are stacked into three separate columns along the *b* axis as shown in Figure 5b and c. The (*R*)- and (*S*)-[PdBr(Hmtbhp)]$^+$ ions are stacked alternately as in **1** and **1H**. Because of the steric hindrance of the [PdBr(Hmtbhp)]$^+$ methyl group, there are no $\pi-\pi$ stacking interactions within the HBA$^-$ columns. The distance between methyl-thio-benzene and pyridine rings within the [PdBr(Hmtbhp)]$^+$ columns (*ca.* 3.37 Å) suggests moderate $\pi-\pi$ interactions. As shown in Figure 5b, each enantiomer is stacked alternately along the column, similarly to **1**, **2**, and **1H**. It is noted that the molecular plane of [PdBr(Hmtbhp)]$^+$ is not parallel to the plane of HBA$^-$ in **4**, showing that the electronic contribution to $\pi-\pi$ stacking is not effective between these units.

On the other hand, the reaction between **2** and H_2BA in 1,4-dioxane afforded the different 1:1 adduct {[PdBr(Hmtbhp)](HBA)·2(1,4-dioxane)} (**5**). Figure 6a shows the hydrogen bond network at 250 K. Complex **5** crystallized in the triclinic $P\bar{1}$ space group. Since the inversion center of the $P\bar{1}$ space group is located on the midpoint between two bromanilic acid molecules, only one crystallographically independent Pd complex and a bromanilic acid molecule are present in the unit cell. Judging from the bond distances around the hydrazone ligand and bromanilic acid shown in Tables 3 and 4, the proton donor H_2BA gave one proton to the Pd complex to form a D···A pair as well as the HBPT assembly **4**. Unlike in the case of **4**, the two D···A pairs are hydrogen-bonded to each other, resulting in the formation of the A···D···D···A type hydrogen bond network. The NH···O hydrogen bond distance between [PdBr(Hmtbhp)]$^+$ and HBA$^-$ is 2.597 Å which is shorter than those of **4** and **7** and slightly longer than that of **6**. Interestingly, the [PdBr(Hmtbhp)]$^+$ and HBA$^-$ units are stacked alternately

(23) Chang, M.; Horiki, H.; Nakajima, K.; Kobayashi, A.; Chang, H.-C.; Kato, M. *Bull. Chem. Soc. Jpn.* **2010**, in press. DOI: 10.1246/bcsj.20100065.

(24) (a) Andersen, E. K. *Acta Crystallogr.* **1967**, *22*, 188–191. (b) Andersen, E. K. *Acta Crystallogr.* **1967**, *22*, 196–201. (c) Ishida, H.; Kashino, S. *Acta Crystallogr., Sect. C* **1999**, *55*, 1149–1152.

(25) Kuleshova, L. N.; Zorkii, P. M. *Acta. Crystallogr., Sect. B* **1981**, *37*, 1363–1366.

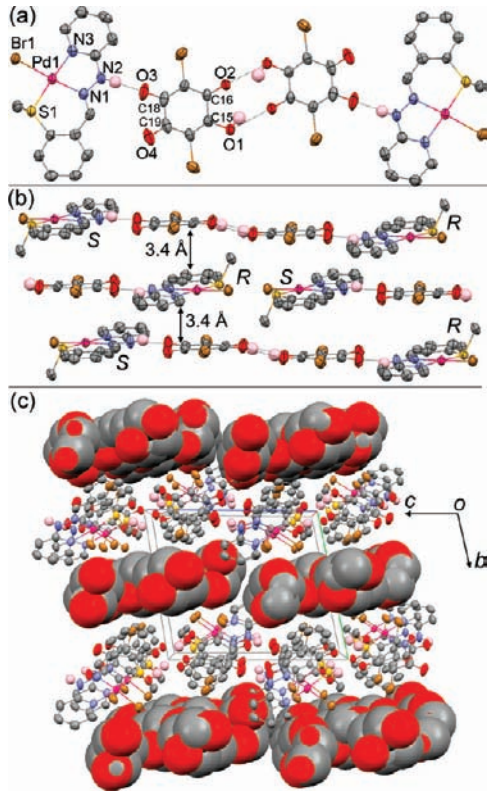

Figure 6. (a) A-D-D-A type hydrogen bond network, (b) stacking structure, and (c) packing diagram of **5** along the *a* axis with thermal vibrational ellipsoids at the 50% probability level. 1,4-Dioxane molecules are shown as space filling models. Dotted lines represent hydrogen bonds. Carbon-bound hydrogen atoms are omitted for clarity.

along the *a* axis with the *ca.* 3.4 Å intermolecular distances between the methyl-thio-benzene or pyrizine rings of [Pd-Br(Hmtbhp)]$^+$ and HBA$^-$ as shown in Figure 6b. This suggests the intermolecular $\pi-\pi$ stacking interaction between these proton donor and acceptor. The electronic absorption band appeared at longer wavelengths than those of **4** and **6** but shorter wavelengths than that of **7**, probably due to the alternately stacking manner and $\pi-\pi$ stacking interaction between the proton donor and acceptor. It should be noted that the solvated 1,4-dioxane molecules were not hydrogen-bonded to any other molecules and formed the layers on the *ac* plane as shown in Figure 6c.

3.3.2. 2:1 Assembly of [PdBr(mtbhp)] and H_2BA. The reaction between deprotonated form **2** and H_2BA in a 1:1 molar ratio in acetonitrile in the presence of 10 equiv of pyrazine afforded crystals of [PdBr(Hmtbhp)]$_2$(BA) (**6**). Figure 7a shows the hydrogen bond network of **6** at 250 K. Complex **6** crystallizes in the monoclinic *C*2/*c* space group. There are no acetonitrile or pyrazine molecules in the crystal. It is noteworthy that two crystallographically independent [PdBr(mtbhp)] units are observed, meaning that the structural features of these two molecules are different. As judged from the bond distances and angles of the hydrazone ligand shown in Table 2, each [PdBr(mtbhp)] unit can accept one proton from H_2BA to form an A···D···A structure. Each structural component is stacked along the *b* axis in the same manner as that in HBPT assembly **4** and protonated complex **1H**. Within the [PdBr(Hmtbhp)]$^+$ columns, the (*R*)- and (*S*)-enantiomers are stacked alternately along the column (Figure 7b). Similar to **4**, the steric hindrance of the methyl group prevents the bromanilates from forming $\pi-\pi$ stacking interactions within bromanilate columns. Since

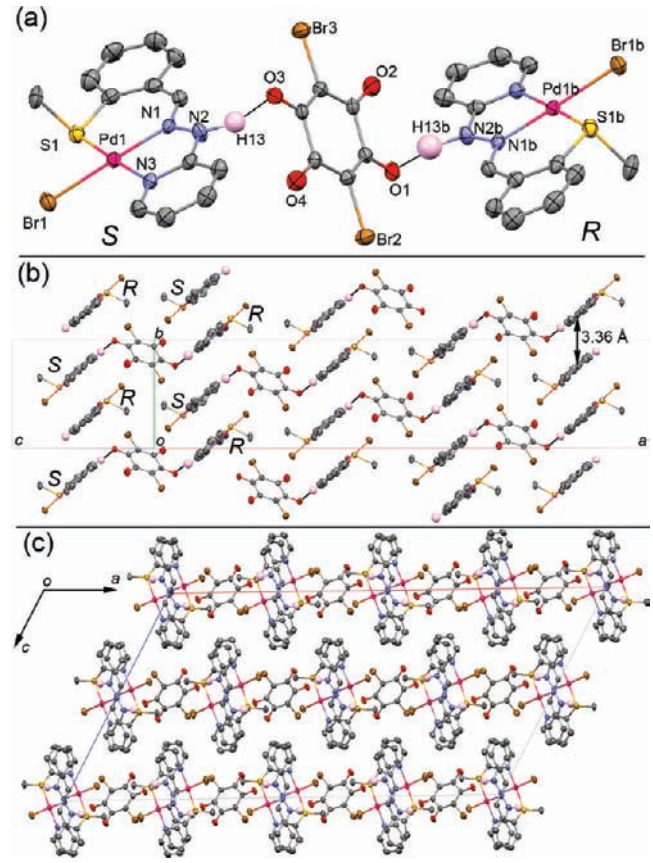

Figure 7. (a) A-D-A type hydrogen bond network, (b) stacking structure, and (c) packing diagram of **6** at 250 K along the *b* axis with thermal vibrational ellipsoids at the 50% probability level. Dotted lines represent hydrogen bonds. Carbon-bound hydrogen atoms are omitted for clarity.

the torsion angles between [PdBr(Hmtbhp)] and bromanilate molecular planes are about 72°, the electronic interaction between these units is thought to be very weak. Distances between methyl-thio-benzene and pyridine rings within [Pd-Br(Hmtbhp)]$^+$ columns (*ca.* 3.36 Å) in **6** are slightly shorter than those in **4**, suggesting relatively stronger $\pi-\pi$ interactions. This difference was confirmed in the diffuse reflectance spectra of **4** and **6**, which show that the absorption band around 600 nm of **6** shifted to longer wavelengths by about 26 nm compared to that of **4** (see Figure S4). It should be noted that the observed bromanilate C=O bond lengths (*ca.* 1.27 Å) do not match those of HBA$^-$ or those of BA^{2-} (*ca.* 1.243 Å) (Table 3), suggesting that the two protons, H13 and H13b, may be disordered between the hydrazone N-site and the bromanilate O-site. As shown in Table 4, the NH···O hydrogen bond distances between bromanilate and [PdBr(Hmtbhp)]$^+$ units are shorter than those in the (Chloranilic acid)(1,2-Diazine)$_2$ proton-transfer complex (2.615 Å) in which hydrogen bond protons can migrate in the solid state.[24b] In fact, the hydrazone N2−H bond distances in two [PdBr(Hmtbhp)]$^+$ units whose hydrogen atoms have been refined isotropically are much longer (1.11(6) and 1.18(7) Å) than the normal value of the N−H bond (*ca.* 0.85 Å). Thus, hydrogen bond protons are expected to migrate between bromanilate and hydrazone units.

To gain more insight about the proton migration, single-crystal X-ray diffraction measurements at lower temperature were conducted for HBPT assembly **6**. Crystallographic parameters obtained at 110 and 150 K are shown in Table 1. At these temperatures, the space groups were similar to that

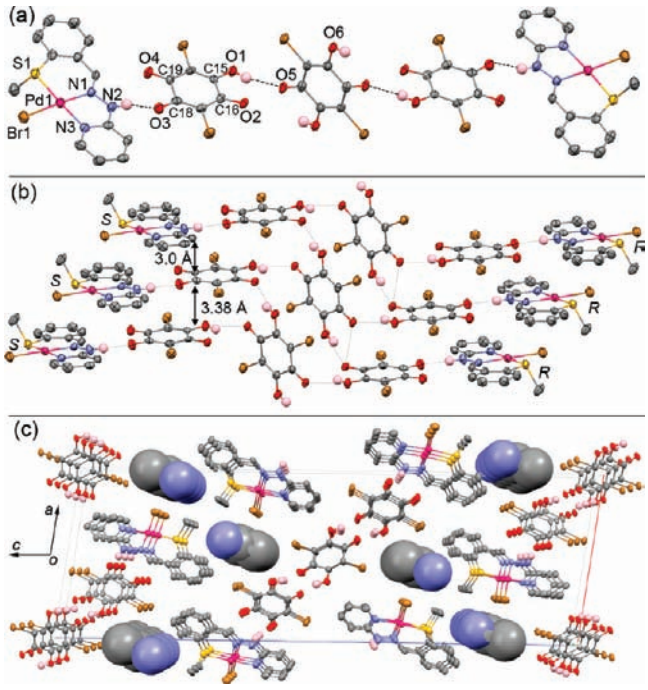

Figure 8. (a) A-D-D-D-A type hydrogen bond network, (b) stacking structure, and (c) packing diagram of **7** at 150 K along the *b* axis with thermal vibrational ellipsoids at the 50% probability level. Acetonitrile molecules are shown as space filling models. Dotted lines represent hydrogen bonds. Carbon-bound hydrogen atoms are omitted for clarity.

obtained at 250 K and the molecular structures were almost the same. However, it may be noteworthy that the N2−C8 bond in the (*R*)-enantiomer shortened slightly with decreasing temperature (see Table 2) and was closer to that of deprotonated form **1** than that of protonated form **1H** at 110 K. The hydrogen bond distance between the bromanilate and (*S*)-[PdBr(Hmtbhp)]$^+$ unit was about 0.017 Å shorter than that between the bromanilate and (*R*)-[PdBr(Hmtbhp)]$^+$ unit at 250 K. At 110 K, these two hydrogen bond distances were the same within experimental error, implying that the electrostatic potential is affected by temperature for the proton. In fact, the N2b−H13b bond was found to lengthen by about 0.5 Å with decreasing temperature, allowing the H13b proton to attach to the bromanilate at 110 K. The N2−H13 bond length also lengthened with decreasing temperature, and the H13 proton was located at the midpoint of the N2···O3 hydrogen bond at 110 K. In addition, the IR spectrum of **6** displayed an absorption band corresponding to the ν(O−H) mode at 3200 cm^{-1} below 150 K (see below). These results suggest that at least one proton can move in the hydrogen bond depending on temperature.

3.3.3. 2:3 Assembly of [PdBr(mtbhp)] and H_2BA. The reaction between the deprotonated form **2** and H_2BA in acetonitrile solution afforded the 3:2 adduct {[PdBr(Hmtbhp)]$_2$(HBA)$_2$(H$_2$BA)·2CH$_3$CN} (**7**) as crystals. It is noteworthy that the reaction conditions of this HBPT assembly were almost the same as those for **4** except for the solvent. Figure 8a shows the hydrogen bond network of **7**, which consists of two [PdBr(Hmtbhp)]$^+$ ions, two HBA$^-$ ions, and one neutral H_2BA molecule. HBPT assembly **7** crystallizes in the monoclinic $P2_1/n$ space group. The bond lengths and angles of the hydrazone and pyridine parts are very close to those of protonated form **1H**, indicating that [PdBr(mtbhp)]$^+$ accepts one proton from the bromanilic acid to form a D···A pair. In addition, the bromanilic acid that is hydrogen-bonded to [PdBr(Hmhtbp)]$^+$ exhibits three shorter C═O bonds and one longer C−O bond, in close agreement with typical values for HBA$^-$ (Table 3). Interestingly, these two D···A pairs are bridged by two hydrogen bonds between one H_2BA molecule and two HBA$^-$ units to form an A···D···D···D···A type hydrogen bond network (Figure 8a). The bridging H_2BA molecule is located at the inversion center and has two shorter C═O (1.229 Å) and two longer C−O bonds (1.319 Å), consistent with its neutrality. As shown in Figure 8b, structural components [PdBr(Hmtbhp)]$^+$, HBA$^-$, and H_2BA are stacked separately. Interestingly, the (*R*)- and (*S*)-[PdBr(Hmtbhp)]$^+$ enantiomers are also stacked separately unlike in HBPT assemblies **4** and **6**. The NH···O hydrogen bond distance between [PdBr(Hmtbhp)]$^+$ and HBA$^-$ is 2.673(5) Å, in close agreement with that in the 55DMBP−H_2CA complex (2.683 Å),[14c] which exhibits a proton-transfer-driven dielectric phase transition in the hydrogen bond. This result implies that the proton between [PdBr(Hmhtbp)]$^+$ and HBA$^-$ may move in the hydrogen bond as a result of some external stimuli such as light, electric field, and temperature. In contrast, the hydrogen bond distance between HBA$^-$ and H_2BA (2.827(5) Å) is significantly longer than the other hydrogen bond distances in this HBPT assembly. The planar [PdBr(Hmtbhp)]$^+$ and HBA$^-$ units are in the same plane whereas the torsion angle between HBA$^-$ and H_2BA molecular planes is very close to 90°, suggesting that the $\pi-\pi$ stacking-induced electronic interactions are effective between [PdBr(Hmtbhp)]$^+$ and HBA$^-$ units but ineffective between HBA$^-$ and H_2BA units. Intermolecular distances within columns show moderate $\pi-\pi$ interactions within HBA$^-$ columns (*ca.* 3.38 Å) but relatively weak $\pi-\pi$ interactions in [PdBr(Hmhtbp)]$^+$ and H_2BA columns (over 3.45 Å). Interestingly, Figure 8b displays significantly short $\pi-\pi$ interactions (*ca.* 3.0 Å) between [PdBr(Hmhtbp)]$^+$ and HBA$^-$ units located above the lower [PdBr(Hmhtbp)]$^+$ molecular plane. The absorption band observed for **7** in the solid state diffuse reflectance spectrum appeared at a longer wavelength compared to **4**, **5**, and **6** (see Figure S4). Considering that $\pi-\pi$ interactions between adjacent HBA$^-$ units are only effective in **7**, the absorption band observed at longer wavelengths (around 650 nm) is attributable to the intermolecular charge transfer transition from HBA$^-$ to [PdBr(Hmhtbp)]$^+$ or the intramolecular $\pi-\pi^*$ transition in HBA$^-$, which is stabilized by the intermolecular $\pi-\pi$ interactions. Acetonitrile molecules also form a 1-D channel along the *b* axis but do not contribute to the hydrogen bond network of this HBPT assembly.

3.4. Proton Migration in the Solid State. The crystal structures of HBPT assemblies **4**, **5**, **6**, and **7** revealed that hydrogen bonds between [PdBr(Hmtbhp)]$^+$ and HBA$^-$ depend on what kind of molecule is hydrogen-bonded to the remaining bromanilate OH group in these assemblies (Table 4). As discussed above, the NH···O hydrogen bond distances (2.577−2.653 Å) suggest that the hydrogen-bonded proton can move toward the O-site of the bromanilate in **6** to form an O−H···N hydrogen bond at low temperature. Proton migration was therefore examined in **6** using IR spectroscopy, one of the most powerful techniques for investigating this phenomenon in hydrogen bonds.[26] Figure 9 shows IR spectra of **6** at various temperatures. Unlike assemblies **4**, **5**, and **7** (see Figure S5), assembly **6** exhibited a very broad band around 2400 cm^{-1} at 300 K. The energies of the stretching modes of N−H and O−H bonds are

(26) (a) Somorjai, R. L.; Hornig, D. F. *J. Chem. Phys.* **1962**, *36*, 1980–1987. (b) Hadzi, D.; Bratos, S. In *The Hydrogen Bond*; Schuster, P.; Zundel, G.; Sandorfy, C., Eds.; North-Holland Publishing Co.: Amsterdam, 1976; Vol. 2, p 565.

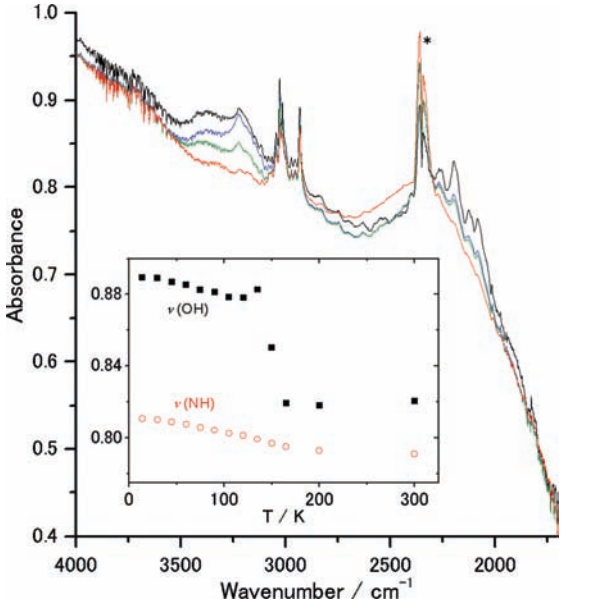

Figure 9. Temperature dependent IR spectra of assembly **6** in the 4000−1700 cm^{-1} region. Red, green, blue, and black lines represent spectra at 300, 150, 135, and 14 K, respectively. Inset: temperature dependent absorbance of the ν(O−H) mode (3218 cm^{-1}) (black square) and ν(N−H) mode (2282 cm^{-1}) (red circle). The marked sharp peak at 2360 cm^{-1} is attributed to the vibration of CO_2 in the air.

known to strongly depend on the hydrogen bond distance. Specifically, the stronger the hydrogen bond, the lower the energy of these bands. With the consideration that the hydrogen bond distance between [PdBr(Hmtbhp)]$^+$ and HBA$^-$ increases according to the order **6** < **5** < **4** < **7** (see above), the broad band around 2400 cm^{-1} observed for **6** is probably attributed to the ν(N−H) mode, which would be remarkably weakened upon hydrogen bond formation. In fact, the deuterated assembly [PdBr(Dmtbhp)]$_2$(BA) (**6D**) showed the broad absorption band attributable to the ν(N−D) mode at around 1830 cm^{-1} (see Figure S6). Although spectra measured above 150 K were almost identical to the spectrum obtained at 300 K, a drastic but reversible spectral change occurred below 150 K, resulting in the appearance of a new absorption band assigned to the ν(O−H) mode around 3200 cm^{-1}. The appearance of this mode suggests that the proton moves from the [PdBr(Hmtbhp)]$^+$ N site to the bromanilate O-site. On the other hand, the ν(N−H) mode around 2400 cm^{-1} was still observed below this temperature (see inset, Figure 9). These results are consistent with X-ray diffraction observations indicating that only one of the two [PdBr(Hmtbhp)]$^+$ units gives a proton to the bromanilate at 110 K. In other words, one proton moves to the bromanilate O-site to form [PdBr(mtbhp)]···HBA$^-$···[PdBr(Hmtbhp)]$^+$ below 150 K (Scheme 1). The pK_a values of bromanilic acid (pK_{a1} = 0.80, pK_{a2} = 3.10)[27] indicate that the proton donating ability of the monoanionic bromanilate is comparable to that of protonated form **1H**. The reason why the proton moved from the hydrazone N-site to the bromanilate O-site with decreasing temperature may be the shrinkage of the crystal accompanied by a change in hydrogen bond distance.

3.5. Vapochromism Derived from the Rearrangement of the Hydrogen Bond Network. We have found that HBPT assembly **7** exhibits an interesting vapochromic behavior toward

(27) Wallenfels, K.; Friedrich, K. *Chem. Ber.* **1960**, *93*, 3070–3082.

Scheme 1. Schematic Representation of Proton Transfer in HBPT Assembly **6**[a]

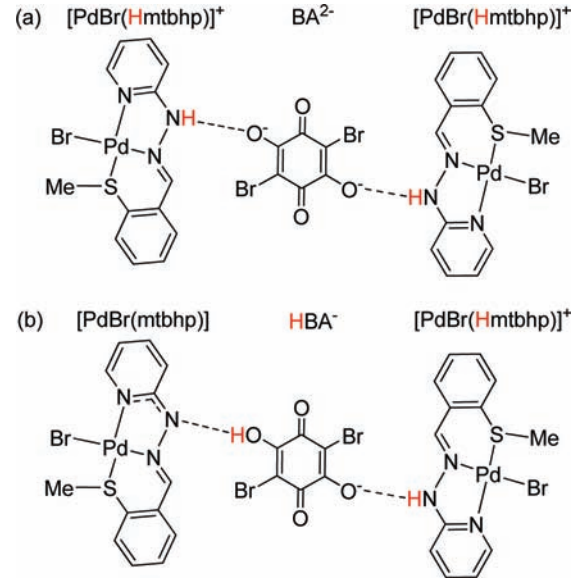

[a] (a) Two-proton-transfer state above 150 K. (b) One-proton-transfer state below 150 K.

organic solvent vapors and that this behavior is deeply related to the hydrogen bonding ability of vapor molecules. We therefore examined this behavior in detail.

As mentioned above, acetonitrile molecules form a 1-D channel along the *b* axis in HBPT assembly **7**. Thermogravimetric analysis revealed that these solvent molecules were easily removed by heating at 373 K in an Ar atmosphere. This acetonitrile removal resulted in a guest-free assembly (**8**) and was accompanied by a significant color change from dark red to reddish-purple (see Figure S7). Elemental analysis and an IR spectrum of **8** also indicated that the acetonitrile was completely removed (aee Figure S8). Interestingly, the original color of **7** was recovered after exposing **8** to acetonitrile vapor at room temperature, suggesting that HBPT assembly **8** is a vapochromic material that can adsorb acetonitrile vapor reversibly. In order to clarify this behavior in detail, UV−vis diffuse reflectance spectra of assembly **8** exposed to several organic vapors were measured. As shown in Figure 10, the acetonitrile-bound assembly (**7**) exhibits a broad absorption band around 650 nm that shifts to shorter wavelengths by about 47 nm upon acetonitrile removal. After exposing **8** to methanol, ethanol, and 1,4-dioxane (*p*-DO) vapors, the absorption band underwent a red shift of about 26, 10, and 64 nm, respectively. On the other hand, exposure to dimethylformamide (DMF), pyridine (Py), dimethylacetoamide (DMA), and dimethylsulfoxide (DMSO) vapors caused the absorption band of **8** to shift to shorter wavelengths by about 16, 32, 45, and 45 nm, respectively.

To confirm whether this vapochromic behavior originates from structural transformations induced by vapor adsorption or not, powder X-ray diffraction (PXRD) patterns were measured. Figure 11 shows the PXRD patterns of **8** exposed to several organic vapors for 2 days. Acetonitrile removal significantly changed the PXRD pattern of **7**, suggesting that the crystal lattice of **7** is not robust enough to retain its structure without the acetonitrile molecules. The original pattern of **7** was recovered after exposing **8** to acetonitrile vapor, showing that HBPT assembly **8** is vapochromic. PXRD patterns obtained after exposing **8** to other organic vapors differed from each other,

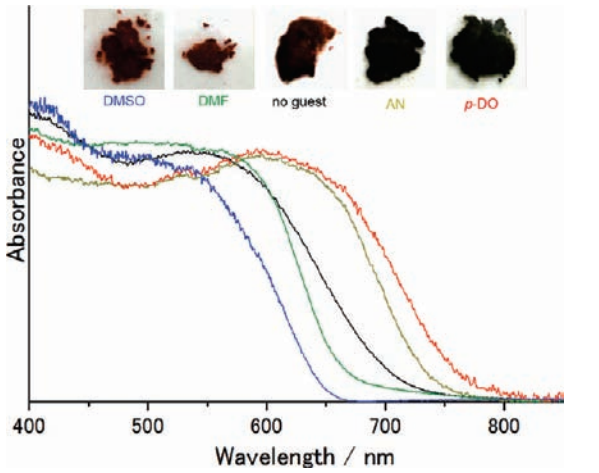

Figure 10. UV−vis diffuse reflectance spectra of **8** after exposure to several organic vapors for 2 days at room temperature. The black solid line shows the spectrum of the guest-free assembly (**8**). Red, brown, green, and blue solid lines represent the spectra of **8** after exposure to 1,4-dioxane (*p*-DO), acetonitrile (AN), dimethylformamide (DMF), and dimethylsurfoxide (DMSO), respectively.

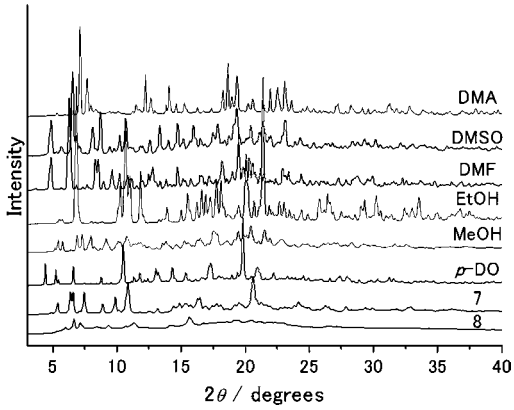

Figure 11. Powder X-ray diffraction patterns of **8** before and after exposure to several organic vapors for 2 days at room temperature.

indicating that the adsorption of these vapors transformed the structure of **8**. It is noteworthy that the PXRD pattern of **8** changed in one step in the presence of acetonitrile vapor but in two steps under exposure to *p*-DO vapor (see Figure S9).

To gain more information about the vapochromic behavior of **8**, IR spectral changes caused by the exposure of **8** to organic vapors were measured. As shown in Figure 12, the vibration modes of bound vapor molecules were observed for each vapor, indicating that the vapochromic behavior of **8** originates from structural transformation induced by vapor adsorption. The band observed at 3178 cm^{-1} corresponding to the ν(O−H) mode of H_2BA was observed for both **8** and **7**, suggesting that the A···D···D···D···A type hydrogen bond network is retained after acetonitrile removal. Assembly **8** showed a new broad absorption band in the 2800−2400 cm^{-1} region when exposed to DMF, DMSO, DMA, and Py vapors, but not to EtOH, acetonitrile, and *p*-DO vapors. Additionally, the ν(O−H) mode of H_2BA observed at 3178 cm^{-1} for **8** clearly disappeared after exposure to DMF and DMSO vapors. As discussed above, the energies of N−H and O−H vibration modes are known to strongly depend on hydrogen bond strength. Taking into account the fact that the hydrogen bond formed between HBA^- and H_2BA is relatively weaker than the other hydrogen bonds in **7**, a vapor molecule that can form a stronger hydrogen bond than

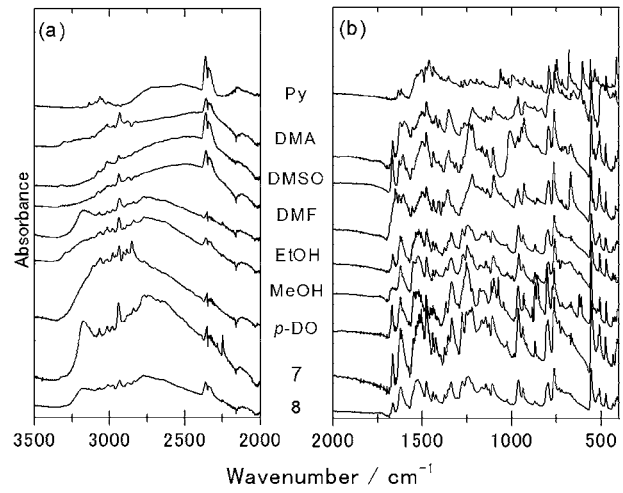

Figure 12. IR spectra of **8** before and after exposure to several organic vapors for 2 days at room temperature.

Table 6. Vapochromic Response of HBPT Assembly **8** and Donor and Acceptor Numbers

Vapor	DN[a]	AN[a]	Vapochromic shift/nm
1,4-dioxane (*p*-DO)	14.8	10.8	64
acetonitrile (AN)	14.1	18.9	47
methanol (MeOH)	19.0	41.3	26
ethanol (EtOH)	22.9	37.1	10
dimethylformamide (DMF)	26.6	16.0	−12
pyridine (Py)	33.1	14.2	−32
dimethylacetoamide (DMA)	27.8	13.6	−45
dimethylsurfoxide (DMSO)	29.8	19.3	−45

[a] See ref 28.

H_2BA will adsorb and insert itself between HBA^- and H_2BA to form a more stable A···D···S type hydrogen bond with the HBA^- OH group. In fact, the ν(S═O) mode of adsorbed DMSO was observed at 1008 cm^{-1} when assembly **8** was exposed to DMSO vapor, which is a *ca.* 42 cm^{-1} shift to lower energy compared to liquid DMSO. Likewise, the ν(C═O) modes observed for adsorbed DMF (1604 cm^{-1}) and DMA molecules (1600 cm^{-1}) also shifted to lower energy by about 70 and 46 cm^{-1} compared to the liquids, respectively. In addition, TG analysis for **8** after exposure to DMF vapor for 1 day revealed that the assembly **8** can adsorb about 2 mol·mol^{-1} DMF vapor (see Figure S10). These results provide more evidence for the contribution of the adsorbed vapor molecules to the hydrogen bond network. Thus, the bands observed within 2800−2400 cm^{-1} after exposing **8** to DMSO, DMF, DMA, and Py vapors correspond to the stretching mode of the HBA^- O−H bond whose strength changes upon vapor adsorption. In contrast, vapor molecules like acetonitrile and *p*-DO that cannot form such a strong hydrogen bond will adsorb without inserting itself between HBA^- and H_2BA. Table 6 shows the donor and acceptor numbers of solvent molecules and the observed chromic shift induced by the vapor molecules. Vapochromic shifts observed for **8** seem related to the donor and acceptor numbers of the vapor molecules. Vapors that make the absorption band around 600 nm of **8** shift to longer wavelengths have relatively small donor numbers and *vice versa*. Molecules with a large donor number and a small acceptor number are known to be good proton acceptors. Thus, this tendency suggests that the hydrogen bonding ability of the vapor is deeply related to the vapochromic behavior of HBPT assembly **8**. In other words,

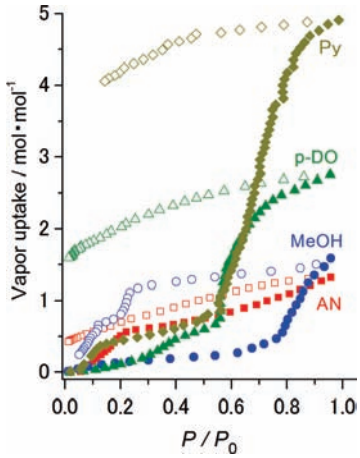

Figure 13. Adsorption isotherms obtained for acetonitrile (red square), methanol (blue circle), 1,4-dioxane (green triangle), and pyridine (yellow diamond) vapor in **8**. Closed and open symbols represent the adsorption and desorption processes, respectively.

the hydrogen bonding mode of **8** was thought to change from the A···D···D···D···A type to the A···D···S type by adsorbing a solvent vapor with a high donor number, but not a vapor with a low donor number and/or a high acceptor number. Actually, in the crystal structure of **4**, the adsorbed acetone molecule has moderate donor (17.0) and acceptor numbers (12.5) and forms a hydrogen bond with the HBA^- OH group. In addition, the diffuse reflectance spectrum of **8** observed after exposure to DMSO vapor was very similar to that of **4** (see Figure S11) in which the $\pi-\pi$ stacking interactions within HBA^- columns are not effective. These results suggest that the vapochromism of HBPT assembly **8**, induced by vapors with high donor and low acceptor numbers, may originate from structural transformations involving significant changes in the hydrogen bond network and $\pi-\pi$ stacking within each structural component. Although there are many reports about vapochromism, to the best of our knowledge, assembly **8** is the first vapochromic proton-transfer complex comprised of proton donor and acceptor molecules and its behavior reflects the hydrogen bonding ability of the vapor.

3.6. Vapor Adsorption Property of the Vapochromic HBPT Assembly 8. As discussed above, HBPT assembly **8** exhibits a vapochromic behavior that strongly depends on the proton accepting ability of the vapor. The vapor recognition ability of **8** was therefore analyzed from the viewpoint of the adsorption property of the vapor. If HBPT assembly **8** can recognize the hydrogen bonding capability of the vapor, the adsorption property may reflect a difference in this capability.

Figure 13 shows the adsorption isotherms of the acetonitrile, *p*-DO, MeOH, and pyridine vapor of **8**. Before each measurement, the sample was dried at 373 K under vacuum to remove the adsorbed acetonitrile from **7**. Although guest-free assembly **8** could adsorb these four vapors, the adsorption profiles for each vapor were significantly different. The adsorption process of acetonitrile vapor proceeded in two steps: after a first adsorption at low pressure (below $P/P_0 = 0.22$, *ca.* 0.56 mol·mol^{-1}), the isotherm gradually reached a saturation point at 1.2 mol mol^{-1}, which corresponds to the number of adsorbed acetonitrile molecules in **7**. Because the PXRD pattern of **8** changed in one step in the presence of acetonitrile vapor (see above), half of the amount of acetonitrile used to reach saturation may be enough to transform **8** into **7**. The adsorption process of *p*-DO vapor was more complicated than that for acetonitrile vapor. After a small adsorption (*ca.* 0.67 mol mol^{-1}) below $P/P_0 = 0.54$, the isotherm showed a sudden increase in vapor uptake at $P/P_0 = 0.54$ and reached a saturation point (2.7 mol mol^{-1}) that was remarkably larger than that for acetonitrile adsorption. This difference in saturation points between acetonitrile and *p*-DO vapors may be related to the number of hydrogen bonding sites in the vapor molecule. The adsorption profile for pyridine vapor, which has a larger donor number than the other three vapors, is similar to that for *p*-DO vapor. The pyridine vapor was first adsorbed around $P/P_0 \approx 0.1$ (adsorbed amount ~0.5 mol mol^{-1}), and then the adsorbed amount was increased rapidly above $P/P_0 = 0.55$. Below $P/P_0 = 0.55$, the adsorption process was similar to that of acetonitrile vapor although pyridine occupies a larger molecular volume than acetonitrile. The saturation point for pyridine vapor was 4.91 mol mol^{-1}, which is significantly larger than that for other vapors. This larger adsorption amount may originate from the high basicity of pyridine. No steep decrease was observed during the desorption process, even at vapor pressures as low as 0.14 P/P_0, suggesting that the pyridine vapor molecules are tightly bound to the crystal lattice due to the potential formation of hydrogen bonds with HBA^- or H_2BA. The adsorption profile obtained for MeOH vapor, which has a larger acceptor number, was very different from the other organic vapors. Adsorption of the MeOH vapor was observed only at pressures exceeding $P/P_0 > 0.76$, which are remarkably higher than those of acetonitrile, *p*-DO, and pyridine vapors. The saturation amount (about 1.5 mol mol^{-1}) was slightly larger than that for acetonitrile vapor, probably due to the smaller volume of MeOH compared to acetonitrile. During the desorption process, the adsorbed amount slightly decreased to $P/P_0 = 0.26$ first and then in two steps via a narrow plateau region to between 0.12 and 0.18. Considering that no steep decrease in adsorption amount was observed for the other organic vapors, the structure of the adsorbed MeOH was less stable than that of other adsorbed vapor. The EtOH vapor adsorption isotherm of **8** revealed the saturation amount (0.55 mol mol^{-1}) was quite smaller by about one-third than that of MeOH (see Figure S12). This result might be consistent with the smaller vapochromic shift for EtOH vapor.

As discussed above, the adsorption behavior of **8** clearly reflects the proton donating/accepting ability of the vapor. Essentially, HBPT assembly **8** can adsorb proton accepting vapors with a large donor number more easily than proton donating vapors with a large acceptor number. This may be due to the fact that assembly **8** consists of a neutral H_2BA molecule and a hydrogen bond network involving $[PdBr(Hmtbhp)]^+$, HBA^-, and H_2BA. In other words, proton accepting molecules can easily form strong hydrogen bonds with HBA^- or H_2BA in HBPT assembly **8** to form stable vapor-bound structures.

4. Conclusion

We have synthesized a new series of [MX(mtbhp)] metal-hydrazone complexes, which exhibit a reversible protonation/deprotonation reaction ($[MX(mtbhp)] + H^+ \rightleftharpoons [MX(Hmtbhp)]^+$) in solution (Hmtbhp = 2-(2-(2-(methylthio)benzylidene)hydrazinyl)pyridine; M = Pd^{2+}, X = Cl^- for **1**; M = Pd^{2+}, X = Br^- for **2**; M = Pt^{2+}, X = Cl^- for **3**). Spectroscopic titration measurements revealed that the acid dissociation constants of Pd(II) and Pt(II) complexes are 3.6 and 3.3, respectively, almost

(28) Gutmann, V. *The Donor-Acceptor Approach to Molecular Interaction*; Plenum Press: 1978.

independently of the halide bound to the metal ion. By reacting [PdBr(mtbhp)] and bromanilic acid (H_2BA), we have succeeded in synthesizing hydrogen-bonded proton-transfer (HBPT) assemblies, {[PdBr(Hmtbhp)](HBA)·Acetone} (**4**), {[PdBr(Hmtbhp)](HBA)·2(1,4-dioxane)} (**5**), $[PdBr(Hmtbhp)]_2(BA)$ (**6**), and $\{[PdBr(Hmtbhp)]_2(HBA)_2(H_2BA)\cdot 2Acetonitrile\}$ (**7**). In these HBPT assemblies, each structural component was stacked separately along the *b* axis, except for **5** in which the proton donor and acceptor were stacked alternately along the *a* axis. The proton donor H_2BA gave at least one proton to the acceptor [PdBr(mtbhp)] to form the hydrogen-bonded $[PdBr(Hmtbhp)]^+\cdots HBA^-$ pair. The hydrogen bond distance between the $[PdBr(Hmtbhp)]^+$ N-site and the HBA^- O-site strongly depended on the molecule that was hydrogen-bonded to the other bromanilate anion OH group. In assembly **6**, the hydrogen bond distance between $[PdBr(Hmtbhp)]^+$ and bromanilate was short enough to enable proton migration in the hydrogen bond, resulting in the transformation of the two-proton-transfer state $[PdBr(Hmtbhp)]^+\cdots BA^{2-}\cdots[PdBr(Hmtbhp)]^+$ into a one-proton-transfer state $[PdBr(mtbhp)]\cdots HBA^-\cdots[PdBr(Hmtbhp)]^+$ at 150 K. HBPT assembly **7** could release the adsorbed acetonitrile upon heating to 373 K to form guest-free assembly **8**, which was found to be an interesting vapochromic material that recognizes the proton donating/accepting ability of the vapor molecule. Further development of these HBPT assemblies is now in progress.

Acknowledgment. The authors thank Prof. H. Kitagawa (Kyoto University) and Emeritus Prof. R. Ikeda (Univ. of Tsukuba) for enlightening discussions and valuable support for low temperature IR spectral measurements. This work is supported by a Grant-in-Aid for Scientific Research (Photochromoism (No.471)), Young Scientists (B) (19750050), and the Global COE Program (Project No. B01: Catalysis as the Basis for Innovation in Materials Science) from the Ministry of Education, Culture, Sports, Science and Technology (MEXT), Japan.

Supporting Information Available: X-ray crystallographic files in CIF format of **1**, **2**, **1H**, **4**, **5**, **6**, and **7**; diffuse reflectance spectra of **4**, **5**, **6**, and **7**; IR spectra of deuterated and nondeuterated **6**; thermogravimetric analyses of **7** and **8** exposed to DMF vapor; exposure time dependence of PXRD pattern of **7**; UV−vis spectra of **2** and **3** in solution; and EtOH vapor isotherm of **8**. This material is available free of charge via the Internet at http://pubs.acs.org.

JA1063444